

# Interferon-responsive neutrophils and macrophages extricate SARS-CoV-2 Omicron critical patients from the nasty fate of sepsis

Mu Wang<sup>1</sup>, Dingji Zhang<sup>1</sup>, Ting Lei<sup>1</sup>, Ye Zhou<sup>1</sup>, Hao Qin<sup>1</sup>, Yanfeng Wu<sup>1</sup>, Shuxun Liu<sup>1</sup>, Liyuan Zhang<sup>1</sup>, Kaiwei Jia<sup>1</sup>, Yue Dong<sup>1</sup>, Suyuan Wang<sup>1</sup>, Yunhui Li<sup>1</sup>, Yiwen Fan<sup>1</sup>, Liangchen Gui<sup>1</sup>, Yuchao Dong<sup>1</sup>, Wei Zhang<sup>1</sup>, Zhixuan Li<sup>1</sup>, and Jin Hou<sup>1</sup>

<sup>1</sup>Naval Medical University

June 07, 2024

## Abstract

The SARS-CoV-2 Omicron variant is characterized by its high transmissibility, which has caused a worldwide epidemiological event. Yet, it turns ominous once the disease progression degenerates into severe pneumonia and sepsis, presenting a horrendous lethality. To elucidate the alveolar immune or inflammatory landscapes of Omicron critical-ill patients, we performed single-cell RNA-sequencing (scRNA-seq) of bronchoalveolar lavage fluid (BALF) from the patients with critical pneumonia caused by Omicron infection, and analyzed the correlation between the clinical severity scores and different immune cell subpopulations. In the BALF of Omicron critical patients, the alveolar violent myeloid inflammatory environment was determined. ISG15<sup>+</sup> neutrophils and CXCL10<sup>+</sup> macrophages, both expressed the interferon-stimulated genes (ISGs), were negatively correlated with Clinical Pulmonary Infection Score (CPIS), while septic CST7<sup>+</sup> neutrophils and inflammatory VCAN<sup>+</sup> macrophages were positively correlated with Sequential Organ Failure Assessment (SOFA). The percentages of ISG15<sup>+</sup> neutrophils were associated with more protective alveolar epithelial cells, and may reshape CD4<sup>+</sup> T cells to the exhaustive phenotype, thus preventing immune injuries. The CXCL10<sup>+</sup> macrophages may promote plasmablast/plasma cell survival and activation as well as the production of specific antibodies. As compared to the previous BALF scRNA-seq data from SARS-CoV-2 wild-type/Alpha critical patients, the subsets of neutrophils and macrophages with pro-inflammatory and immunoregulatory features presented obvious distinctions, suggesting an immune disparity in Omicron variants. Overall, this study provides a BALF single-cell atlas of Omicron critical patients, and suggests that alveolar interferon-responsive neutrophils and macrophages may extricate SARS-CoV-2 Omicron critical patients from the nasty fate of sepsis.

## 1. INTRODUCTION

The Omicron variant of Severe Acute Respiratory Syndrome Coronavirus 2 (SARS-CoV-2) was detected for the first time in Botswana and South Africa in November 2021, which was characterized by the higher transmissibility, increased immune evasion and less virulence, thus causing pandemic around the world.<sup>1</sup> The initial spike protein of the variant of concern (VOC) Omicron BA.1 harbors 32 drifted mutations as compared to the ancestral pre-Alpha wild-type strain (Hu-1), and this variant varies considerably in the pathogenicity, severity and immune remodeling.<sup>2</sup> Although global coronavirus disease 2019 (COVID-19) vaccination inoculation rate by the end of 2022 had reached a brand-new peak and the metrics had drawn near 87% in China, breakthrough infection of Omicron variant still caused its pandemic spread.<sup>3</sup> In contrast with previous waves dominated by wild-type, GR (D614G), Alpha and Delta variants, the infection of Omicron variant presented lower levels of hospitalization, milder symptoms, and reduced severity.<sup>4</sup> In addition, Omicron variant is five-to-seven fold more infectious to human alveolar type 2 cells than GR (B.1.1.119), Alpha (B.1.1.7) and Delta (B.1.617.2).<sup>5</sup> However, the mortality rate caused by severe or critical Omicron cases seemed higher than its ancestry.<sup>6</sup> Thus, the underlying cell and molecular mechanisms, especially in the lung of Omicron severe or critical cases, need to be further investigated.

Notwithstanding the plethora of literatures that was quickly published in the wake of the initial outbreak, the advantages of single-cell multi-omics to unpack the microenvironmental force that drove the etiology and pathology of COVID-19,<sup>7</sup> the disease characteristics of critical-ill Omicron cohorts, particularly concerning pulmonary inflammation, cellular composition and immunological landscape were not yet understood. As for pre-Alpha and Alpha strains, multipronged single-cell technologies have been applied to obtain immune profiles of peripheral blood mononuclear cells (PBMCs) or the whole blood cells from those patients. The data presented the increased dysfunctional CD14<sup>+</sup>/HLA-DR<sup>lo</sup>/CD163<sup>hi</sup> and CD14<sup>+</sup>/HLA-DR<sup>lo</sup>/S100A<sup>hi</sup> monocytes, dysfunctional neutrophil precursors expressing PD-L1, circulating adaptive NKG2C<sup>+</sup>/CD57<sup>+</sup>/CD56<sup>dim</sup> NK cells, the ratio of expanded CD8<sup>+</sup> effector T cells to effector memory T cells, interferon-alpha (IFN- $\alpha$ ) deficient plasmacytoid dendritic cells (pDCs), and circulating follicular helper T cells in severe cases in contrast to the mild ones.<sup>8-10</sup> Clonal expansions of plasmablasts with no somatic hypermutations, detectable clonal sharing and broadly auto-reactive B cells were found in hospitalized critical COVID-19 patients, consistent with an emerging role for B cell-driven immune pathology.<sup>11</sup> The hyperactivation of T cell subpopulations expressing broad proliferation markers and profound skewed T cell receptor repertoire also emerged in most severe patients with intense lymphopenia.<sup>12,13</sup> What's more, pre-Alpha/Alpha patients' PBMCs were observed to have strong IFN- $\alpha$  responses in almost all cell types in severe cases in comparison to moderate counterparts, and over-activation of IFN pathways might contribute to the immune dysfunction and injury.<sup>11,14</sup> Meanwhile, the literatures of BALF analyses of pre-Alpha/Alpha severe patients were much fewer than those of PBMCs. Previous studies reported that "cytokine storm" is a propulsion of late-stage severe pneumonia where two inflammatory macrophage subsets characterized by *CCL2* / *CCL3* and *FCN1* / *S100A8* caused extensive damage in the lung and vascular tissues.<sup>15</sup> Compared with mild patients from volunteer donors, BALF in severe patients had less alveolar macrophages, NK cells and pDCs, but more FCN1<sup>+</sup> monocytes and monocyte-derived SPP1<sup>+</sup> macrophages, suggesting excessive inflammation by promoting monocyte recruitment and differentiation and, even worse, COVID-19-associated lung fibrosis.<sup>16-18</sup> Naïve phenotype CCR7<sup>+</sup>/CD8<sup>+</sup> T cells were enriched in the BALF of severe patients, while resident memory ZNF683<sup>+</sup>/CD8<sup>+</sup> Trm cells were specific to mild patients and even higher in females than in males.<sup>16,18,19</sup> This point indicated that immature effector T cell response could lead to inefficient viral clearance, and the T cell memory response to resolve the virus was impaired in SARS-CoV-2 severe patients as well, especially in males. Nevertheless, there have been no clearly defined specific immune cells that could serve as definitive diagnostic criteria as to the current clinical practices, and whether these BALF analyses could contribute to the clinical decision-making or are associated with the prognosis of severe COVID-19 patients remain to be elucidated.

One of the most important features of Omicron infection is that elderly patients with hospital-acquired pneumonia (HAP) are more predisposed to deteriorate into sepsis, which is the leading cause of death. These patients usually have bacterial co-infection, diffuse pulmonary damage, acute respiratory distress syndrome (ARDS) or even multiple organ failure.<sup>20-22</sup> To elucidate the alveolar immune or inflammatory landscape of SARS-CoV-2 Omicron, we performed scRNA-seq of the BALF from critical-ill patients during the 2023 Omicron incursion in China. The Clinical Pulmonary Infection Score (CPIS) and Sequential Organ Failure Assessment (SOFA) presenting the disease severity of these critical patients was used to analyze the correlation between the cell populations in the BALF and the development of severe Omicron. Hence, the landscape of immune cells in the lung of severe Omicron patients was presented, and their correlation with disease progression was suggested in this study.

## 2. MATERIALS AND METHODS

### 2.1 Ethic statement

This work on humans was carried out on grounds of the principles manifested in the Helsinki Declaration and its later amendments. Prior ethical approval was granted by the Research Ethics Committee of the First Affiliated Hospital of Second Military Medical University, Shanghai, China. 17 out of 32 patients in this cohort which had been enrolled with SARS-CoV-2 pneumonia were transferred from the emergency department to the ICU ward from December 2022 to January 2023. The written informed consent for BALF

collection and subsequent analyses was offered by a surrogate decision-maker. The research staff did not participate in clinical decisions.

## 2.2 Cohort features

All the 17 critical Omicron patients at the median age of 77 (range, 61-99), received vaccination against SARS-CoV-2 previously. Attending physicians defined disease severity as critical according to the “Diagnosis and Treatment Protocol of COVID-19 (Trial Version 9) revised by China National Health Commission and the National Administration of Traditional Chinese Medicine issued on March 15, 2022. The outcome was judged as a censor if the observation limit had been over a maximum of 60 days post the outset of mechanical intubation. Two censor cases were determined as alive because of the exceeding of the maximum observation limit. The characteristics of the 17 patients were listed in Supporting Information Table S1.

## 2.3 Sample collection and isolation of BALF cells

Bronchoalveolar lavage was operated by virtue of wedging the bronchoscope into a subsegmental bronchus. Lavage was aspirated with 20 mL saline solution. One of the two equal aliquot each sample were resuspended in cooled RPMI 1640 and passed through a 70  $\mu\text{m}$  nylon strainer to remove clumps, debris and phlegm three times. After the lysis of red blood cells, the aliquot was centrifuged to precipitate cells, resuspended and then counted using the Countstar viable cell counter. Dead cells were removed with low-speed centrifugation before single-cell capturing and about  $5 \times 10^6$  living cells was collected per patient.

## 2.4 Isolation of viral cDNA

The other aliquot of BALF sample was diluted using PBS added with 0.1% DTT to remove phlegm. After passing through a 70  $\mu\text{m}$  nylon strainer, this aliquot was centrifuged, and the supernatant was used for RNA extraction using QIAmp Viral RNA Mini Kit (Qiagen, 52904). First strand cDNA synthesis was constructed using SuperScript III One-Step RT-PCR Kit (Thermo Scientific, 12574026).

## 2.5 Single cell capturing, library construction and count matrix generation

Single-cell libraries were constructed according to the manufacture instruction of GEXSCOPE<sup>®</sup> Single Cell Transcriptome Reagents.<sup>23</sup> Briefly, cell suspensions were decanted into microwell chip using the Singleron Matrix<sup>®</sup> Single Cell Processing System. Barcoding beads are subsequently collected from the microwell chip followed by reverse transcription of the mRNA and PCR amplification. The amplified cDNA is then fragmented and ligated with sequencing adapters. The libraries were diluted to 4 nM, and sequenced on Illumina Novaseq 6000 with 150 bp paired end reads. Raw reads were first processed using CeleScope v.1.9.0 (<https://github.com/singleron-RD/CeleScope>) to remove low quality reads with Cutadapt v.1.17 to trim poly-A tail and adapter sequences. Then, STAR v2.6.1a was used to map reads to the reference genome GRCh38 (ensembl version 92 annotation). UMI and gene counts of each cell were acquired with featureCounts v2.0.1 software to generate expression matrix files.

## 2.6 Quality control, dimensionality reduction, batch correction and cell clustering identification

Total droplet was set to a point under the plateau of the barcode rank plot. Ambient RNA as well as empty droplet were rectified with SoupX v.1.2.2. Doublets were detected using scrublet v.0.2.163. Cells with fewer than 100 or more than 15000 unique transcript reads were removed as low-quality cells or potential doublets. CeleScope performed sample quality filtering according to the following three benchmark: (1) `n_genes_by_counts` (the number of genes per barcode); (2) `total_counts` (the UMI number per cell); (3) `percent_mt` (the fraction of counts from mitochondrial genes per barcode). Any cell from which sequencing reads aligned to mitochondrial genes  $> 20\%$  was excluded from further analysis. 193,036 cells were filtered after CeleScope QC to generated a cells-by-genes matrix and 112,926 cells were included in the final analysis. QC results were presented on Supporting Information Table S2.

By means of Seurat v.4.0, “`LogNormalize()`” and “`ScaleData()`” functions were used to eliminate gene expression variance. The top 2,000 variable genes were identified using “`FindVariableFeatures()`” function for PCA analysis. The top 20 principal components were used for dimensionality reduction. To allow the comparison

across different samples within our Omicron dataset, Harmony algorithm was used to integrate the whole expression matrices. Integration anchors using “FindIntegrationAnchors()” function were performed. PCA matrices were fed into “HarmonyMatrix()” function to added an integrated assay to the Seurat object. Louvain clustering was performed on the PCA-reduced data using “FindNeighbors()” and cell cluster annotation was performed using Singleron SynEcoSys database and manual curation based on sing-cell databases such as PanglaoDB, CellMarker and the related literatures. The “FindAllMarkers()” function for initial labelling resulted in the identification of separate cell types.

## 2.7 Differential gene expression analysis and Reactome enrichment

For each subcluster, differentially expressed genes (DEGs) were excavated using Seurat “FindAllMarkers()” function based on Wilcox likelihood-ratio test with default parameters. To control false discovery rate (FDR), the gene with a minimal fraction of 25% for each subcluster with adjusted p-value (q-value) < 0.05 and the  $-\log_2(\text{fold change}) \geq 1$  was considered significant. The Reactome pathway activity scores of individual cells were calculated by AUCell v.1.22.0 according to Reactome database. Based on hypergeometric distribution, pathways with a median fold change > 3 and an adjusted p-value (q-value) < 0.01 were perceived as significantly differentially expressed.

## 2.8 Correlation analysis

For single-cell based correlation analysis, we calculated the cellular proportions of each immune cell subcluster on grounds of their fractions in the corresponding main cell types in each sample. The correlation of each selected cell subcluster with different CPIS and SOFA grades and the correlation of each cell subcluster with every other subcluster was calculated using Spearman correlation coefficient assay.

## 2.9 Trajectory inference

The R package Monocle2 v.2.28.0 was utilized to quest pseudotime lineages development for neutrophils and macrophages separately. Highly-variable genes (HVGs) were used to sort cells in order of spatial-temporal differentiation. Reversed DDTree embeddings emptied into Monocle2 with State1 set as a root state. To identify genes that are significantly regulated as the cells differentiate along the cell-to-cell distance trajectory, we used the “differentialGeneTest()” function to explore the gene expression level. Trajectory-specific genes were grouped into two clusters for N03, three clusters for M06 and three clusters for M01 based on similar expression trend.

## 2.10 Integration of datasets across meta-sample sources

To integrate cells into a shared space between our Omicron dataset and previously reported SARS-CoV-2 datasets, we recovered BALF single-cell transcriptome open-source datasets as validation cohorts of 39 subjects. In brief, Harmony method reintegrated the 39 reference samples with our Omicron dataset into a same principal-component space as above mentioned. All relevant data were downloaded from Gene Expression Omnibus under the accession numbers GSE145926 (S1-S6), GSE167118 (S1-S5, S7-S9), GSE147143 (S1-S3), the archive from EGAS00001004717 (BAL012-016, BAL020-027, BAL031-035, BAL039-040) and the archive <https://doi.org/10.6084/m9.figshare.12436517>, (BIH-CoV-01, BIH-CoV-02).

## 2.11 Visualization

Plotting was performed using ggplot2 v.3.3. Comparisons of significance indicator were visualized using ggsignif v.0.6.0. Heatmaps were generated using pheatmap v.0.12.0. Sankey plots were generated using ggraph v.0.12.0. Figure layouts were pieced together by patchwork v.1.0.1 and Adobe Illustrator cc.2018.

## 2.12 Statistical analysis

Statistical analysis was performed using R v.4.3.1 and GraphPad Prism v.8. For the hypothesis testing, normality was computed firstly using a Shapiro-Wilk test and manual examination of distributions in SPSS Statistics 22. For parameters that exhibited a clear lack of normality, nonparametric tests were used. Regarding to multiple testing, p values were corrected using FDR correction to generate adjusted p values

or q values (Benjamini-Hochberg method). Adjusted p values  $< 0.05$  were considered significant. Two-sided statistical tests were applied in all sample data.

### 3. RESULT

#### 3.1 Study overview

In our study, 17 patients at the median age of 77 at the beginning of 2023 were included. These 17 patients were all critical COVID-19 patients with the infection of SARS-CoV-2 Omicron variant, and all in the respiratory ICU undergoing endotracheal intubation, invasive ventilation, bronchoalveolar lavage, broad-spectrum antibiotics, glucocorticoid impulse, and sedatives (Figure 1A). The severe or critical Omicron infection was diagnosed based on one of the following criteria: (1)  $\text{PaO}_2/\text{FiO}_2$  [?]  $< 300$  mmHg; (2) respiratory failure and invasive mechanical ventilation; (3) combined failure of other organs requiring ICU monitoring; (4) shock.<sup>16</sup> In these patients, 15 of them were male while only two were female, and five male patients thereof survived ultimately while the others met a fatal end. The baseline information of these Omicron critical patients was similar with previous pre-Alpha or Alpha cases that the severe incidence rate is much higher in men than women.<sup>24,25</sup> All patients suffered from severe bacterial pneumonia and ten patients of them combined at least one organ failure. On the day of sampling, their International Normalized Ratio (INR) and C-reactive protein (CRP) values all exceeded the highest threshold, the median percentage of neutrophils in peripheral blood reached 92.15%, and their SOFA scores [?]  $\geq 2$ , indicative of severe sepsis (Supporting Information: Table S1).<sup>26</sup>

We performed scRNA-seq of the BALF cells obtained from these 17 Omicron critical patients, and the BALF of seven patients were collected longitudinally two to three times while the other ten were collected only once. Total 26 BALF samples were then sequenced using Singleron GEXSCOPE<sup>(r)</sup> platform (Figure 1B). None of them have been treated with IFN before, but ten patients have received anti-COVID-19 medicine Paxlovid or Azvudine. The high Omicron viral load was determined by qPCR assay aimed at open reading frame 1ab (ORF1ab) and nucleocapsid protein in the nasopharyngeal swab of these 17 patients on the sampling day (Supporting Information: Table S1).

#### 3.2 The alveolar immune and inflammatory landscape of severe Omicron elucidated by scRNA-seq

To elucidate the alveolar immune and inflammatory landscape of SARS-CoV-2 Omicron critical-ill patients, we sequenced a total of 112,926 cells with an average of 4343 cells per sample and 783 genes per cell (Supporting Information: Table S2). Cellular identities were matched to five kind of main granularity using uniform manifold approximation and projection (UMAP) (Figure 2A). Clustering analysis was manually annotated by querying known lineage genes, presenting 27 distinct clusters composed of neutrophils (*PTPRC*, *CSF3R*), macrophages (*CD68*, *CD163*), epithelial cells (*KRT18*), T cells (*CD3D*), NK cells (*KLRD1*), B cells (*CD79A*, *MS4A1*) and plasma cells (*CD79A*, *JCHAIN*) (Supporting Information: Figure S1A). Overall, we observed an enrichment for neutrophils (82,610) and macrophages (14,644), ranking them as the top two, which suggested the infiltration of myeloid cells in these severe patients (Supporting Information: Figure S1B).

After identifying the main cell lineages, we subjected each lineage to subclusters respectively. In the neutrophil subsets, N01, expressing abounding chemokines and *PI3*, was the most predominant population of neutrophils (Supporting Information: Figure S1C). The percentages of  $\text{CST7}^+$  neutrophils (N02) ranked the second only to N01 (Supporting Information: Figure S1C), and the highly-expressed *S100A8*, *S100A9*, *CXCR2*, *MNDA* and anti-bacterial protein NB1 (*CD177*) in these N02 neutrophils suggested that they were closely related to sepsis (Figure 2B).<sup>7,27,28</sup> N03 expressed a great degree of IFN-stimulated genes (ISGs) (Figure 2B). The  $\text{MMP9}^+/\text{ARG1}^+$  neutrophils (N04), concomitantly expressing *MMP8*, represented an immunosuppressive phenotype with the characteristics of myeloid-derived suppressor cells (MDSCs), immature low-density neutrophils, or developing neutrophils with tertiary granule according to the previous studies (Figure 2B).<sup>9,27,29-31</sup> N05, expressing heat shock protein genes *HSP1A1*, *HSPH1*, *HSP90A* and *HSPA8*, was a neutrophil subset under stress (Figure 2B). The rest of neutrophils were grouped into N06 with no

specific definition (Figure 2B).

In the macrophage subsets, the most predominant is M01 with chemotactical activity (CXCL5, CCL7 and CXCL2) (Figure 2B). M03 expressed *LYZ*, *VCAN* and *FCN1*. M01 and M03 both exhibited a feature of previously reported monocyte-derived macrophages (Figure 2B).<sup>32</sup> GPNMB<sup>+</sup> macrophages (M02) might promote viral invasion as the highly expressed CTSL, a lysosomal cysteine protease, which was suggested to be an ingress medium for SARS-CoV-2 Spike protein (Figure 2B).<sup>33</sup> M04 possessed the characteristics of interstitial macrophages (IMs), expressing the HLA family member genes *HLA-DRA* and *HLA-DRB1*, complement activation genes *C1QA*, *C1QB*, *C1QC*, and post-phagocytic lipid degradation/metabolism gene *APOE*.<sup>34</sup> The expression of maturation markers CD40 and CD80 in M04 suggested its capability of antigen presentation. They also expressed chemokine receptor CCR7 and chemoattractants CCL17, CCL22, representing their ability of chemotactic migration and Th2 response (Figure 2B, Supporting Information: Figure S1D). M05 expressed stress-related genes *HSPB1* and *BAG3*. M06 were characterized by IFN-stimulated genes *CXCL10*, *IFI27* and immunological tolerant gene *VSIG4*. M07 expressed *FABP4*, but not migration genes *ICAM1* and *MARCKS*, manifesting that they were alveolar macrophages (AMs).<sup>16</sup> Its tissue residency and expression of TLR3 indicated the capability of the antiviral innate immune responses (Figure 2B, Supporting Information: Figure S1D). Besides, predominant neutrophils and macrophages, including N01, N02, M01, M02 and M03, exhibited substantial expression of pro-inflammatory chemokines, such as CCL2, CCL3, CCL4L, CCL7, CXCL2, CXCL3 and CXCL5 (Figure 2B), indicating their roles in the progression of cytokine storm in critical Omicron patients.

The lymphocyte group contained only 4,719 cells (Supporting Information: Figure S1B). T02 and T06 were delineated as NK cells in view of their preference in CD94 (*KLRD1*) expression but not CD3D. All subpopulations of T and NK cells exhibited expression of ribonucleoprotein subunit signature genes *RPL13*, *RPL23A* and *RPS29*, suggesting their state of high RNA translation and ribosome metabolism. For T cells, we found a population of CD8<sup>+</sup>/CD127<sup>+</sup> (*IL7R*) T01 with the characteristics of antiviral memory, which might represent the adaptive immune programs after vaccination (Figure 2B).<sup>35,36</sup> Meanwhile, we also observed a subset of CD4<sup>+</sup>/PD1<sup>+</sup> T03 cells exhibiting an exhausted phenotype. T04 was a population of naive T cells. T05 expressed GZMA, GZMB and T cell activating signal CD27, and a subset of CD8<sup>+</sup>/KI67<sup>+</sup> T07 cells displaying a proliferative phenotype (Figure 2B). Of note, in the atlas, T and NK cells were not contributors to the pro-inflammatory cytokine milieu, indicating that the alveolar inflammatory environment in severe Omicron patients was not elicited by T or NK cells. For B cell family, the plasmablasts (PBs) of JCHAIN<sup>+</sup>/KI67<sup>+</sup> B01 and plasma cells (PCs) of JCHAIN<sup>+</sup>/KI67<sup>-</sup> B02 also expressed MZB1, the feature of marginal zone B cells (MZBs), suggesting that the humoral immune response might be present in the alveolar microenvironment of these severe Omicron patients (Figure 2B). However, we did not find several other immune cell subsets, including HLA-DR<sup>lo</sup> monocytes (*CD14*, *FCGR3A*), IFN-deficient pDCs, conventional dendritic cells (cDCs), and NKT cells (*KLRK1*, *KLRB1*), which were observed by previous scRNA-seq of pre-Alpha and Alpha severe cases.<sup>37</sup> Together, the alveolar immune landscape of severe Omicron patients was elucidated by scRNA-seq of the BALF, suggesting the myeloid cells infiltration and lymphopenia in the lung.

### 3.3 High IFN-responsive ISG15<sup>+</sup> neutrophils and CXCL10<sup>+</sup> macrophages were correlated with the alleviation of critical Omicron disease

To examine whether cell composition of the BALF was correlated with the severity of critical Omicron disease, the percentage of each cell subcluster each patient was counted. The global subcluster proportions were normalized by Z-score in row, and their correlations with CPIS or SOFA grades were analyzed (Figure 3A). For CPIS, the number of N03 neutrophils and M06 macrophages in the CPIS low group were significantly higher than their respective counterparts in the CPIS high group (Figure 3B). Moreover, both N03 and M06 numbers were negatively correlated with the CPIS grades (Figure 3C). Thus, high ISG15<sup>+</sup> N03 neutrophils and CXCL10<sup>+</sup> M06 macrophages were correlated with the alleviation of critical Omicron disease.

For the cell subsets correlated with the progression of Omicron disease, we found that chemotactically-active CXCL5<sup>+</sup> M01 macrophages were significantly increased in the CPIS high group, and were positively corrected

with the CPIS grades (Figure 3B, C). Moreover, CST7<sup>+</sup> N02 neutrophils and VCAN<sup>+</sup> M03 macrophages were significantly increased in the SOFA high group, and exhibited a positive correlation with the SOFA scores (Fig 3B, C). Hence, these cell subsets may represent the advanced inflammatory state in the lung of critical Omicron patients.

As ISG15<sup>+</sup> N03 neutrophils and CXCL10<sup>+</sup> M06 macrophages, both of which were correlated with the disease alleviation, the preferred gene expressions in these two cell subsets were then analyzed. As compared to other cell subsets of the BALF, N03 and M06 highly expressed a set of ISGs (Figure 4A), and exhibited the IFN antiviral innate immune function, such as OAS antiviral response, IFN- $\alpha/\beta$  signaling, TRAF3-dependent IRF activation, and ISG15 antiviral mechanism (Figure 4B). These pathways were mediated by a series of upregulated ISGs communally shared by N03 and M06 subsets, such as *ISG15*, *IFIT3*, *IFITM3* and *MX1* (Figure 4C). Protein-protein network analysis also revealed that these commonly upregulated ISGs worked synergistically to participate in antiviral mechanisms (Figure 4D, E).

For epithelial cells, we found that FOXJ1<sup>+</sup> E01 epithelial cells possessed a large number of ion transport and flagella maintenance genes like *SNTN*, *CAPS*, *RSPH1*, together with ciliated epithelial-selective genes *TPPP3* and *TMEM190*, thus were considered as ciliated epithelial cells (Figure 2B).<sup>38</sup> E02 SERPINB3<sup>+</sup> epithelial cells were considered as club-cell-like secretory epithelial cells based on the expression of anti-bacterial immunoglobulin-binding markers like uteroglobin (*SCGB1A1*), *BPIFB1* and *BPIFA1* (Figure 2B).<sup>38</sup> E03 SPRR2A<sup>+</sup> epithelial cells expressed *SPRR2A*, *SPRR3*, *SPRR1B*, and keratinization genes *KRT13* and *KRT17*, which were essential to squamous cell cornification and epidermal differentiation complex (EDC) formation, thus may represent transitional AT1 cells (Figure 2B).<sup>32,39,40</sup> E04 SFTPB<sup>+</sup> epithelial cells exhibited characteristics of AT2 cells with alveolar surfactant protein genes *SFTPB* and *NAPSA* (Figure 2B).<sup>19</sup> Notably, E01, E02, and E03 epithelial cells possessed protective properties against lung injury,<sup>41,42</sup> and their cell proportions were negatively correlated with the inflammation-promotive N01 and N02 neutrophils respectively (Figure 4F). However, E01, E02, and E03 populations exhibited a significant positive correlation with the favorable IFN-responsive N03 ISG15<sup>+</sup> neutrophils (Figure 4G). Besides, the inflammation-promotive monocyte-derived M03 macrophages were negatively correlated with these favorable N03 cells (Figure 4G). Together, high ISG15<sup>+</sup> neutrophils and CXCL10<sup>+</sup> macrophages, both IFN-responsive, are correlated with the alleviation of critical Omicron disease, and ISG15<sup>+</sup> neutrophils may participate in the epithelial barrier defense.

### 3.4 The chronological manifold of neutrophils and macrophages

We next outlined the latent-time trajectories of neutrophils and macrophages using time-delayed embedding. For neutrophils, PI3<sup>+</sup> N01 neutrophils were assigned as “root cells” in latent time pseudo-ordering, because they accounted for the most proportion of State 1 (Supporting Information: Figure S2A). CST7<sup>+</sup> N02 neutrophils gradually increased over latent time toward State 5, 6, 7 and 8, and presented a reverse trajectory orientation as compared to PI3<sup>+</sup> N01 neutrophils, which was toward State 1, 2, 3 and 4, bifurcating from node 1 (Supporting Information: Figure S2A). MMP9<sup>+</sup>/ARG1<sup>+</sup> N04 neutrophils mainly oriented toward the developmental direction like N02 neutrophils, and reached their apex at State 5.

For macrophages, recovery from inferred latent time, VCAN<sup>+</sup> M03 macrophages progressively decreased as they evolved toward the terminal state, and appeared to be an origin of classic monocyte-derived macrophages (Supporting Information: Figure S2A). When embedding macrophage lineages, CXCL5<sup>+</sup> M01 macrophages appeared to proceed from M03 macrophages, and developed toward the State 2, 3 and 4 (Supporting Information: Figure S2A). GPNMB<sup>+</sup> M02 macrophages and C1QC<sup>+</sup> M04 macrophages developed through the node 4 and toward the terminal State 7, 8 and 9, indicating that these two subsets are terminally developed macrophages. M02 and M04 macrophages expressed *GPNMB*, *CTSB* and *SPP1*, suggesting that they were M2 polarized (Supporting Information: Figure S2A).<sup>16,43</sup> These data may suggest that the alveolar macrophage polarization was processing from circulating monocytes to pro-inflammatory macrophages and then to terminally reparative pro-fibrotic macrophages.

It was observed that the quantities of ISG15<sup>+</sup> N03 neutrophils and CXCL10<sup>+</sup> M06 macrophages remained

constant over pseudotime passage from beginning to end. This may suggest that these two IFN-responsive subsets maintained a stable presence throughout the course of Omicron sepsis. However, we noticed that the peak expression of ISGs in both subsets occurred in the mid-to-late part of the pseudotime axis, which is opposite to that of M01, expressing inflammatory genes and peaking in the early-to-mid and declining in the late stage (Supporting Information: Figure S2B). Hence, in a chronological perspective, the myeloid pseudo-temporal manifold seemed to progress toward a direction of eliminating viral infection and inflammatory resolution.

### 3.5 The signals from CXCL10<sup>+</sup> macrophages to B cells and ISG15<sup>+</sup> neutrophils to CD4<sup>+</sup> T cells

To further illustrate the communications of macrophages and neutrophils with other immune cells, we analyzed the cellular connectomes. Subpopulation intercourse strength was plotted to demonstrate the cell-cell interactions. We divided outgoing-incoming signal patterns into three major parts, including secreted signals, cell-cell contacts, and extracellular matrix (ECM)-receptors (Supporting Information: Figure S3A, B). Network topology of six main signal families with edges filtered to those where neutrophils and macrophages functioned as senders revealed the characteristic cell to cell communications (Supporting Information: Figure S3C).

For macrophages, we found that CXCL5<sup>+</sup> M01 macrophages showed massive inflammatory factors epitomized by IL-1 $\beta$  and CXCL2/8, and secreted signals to CST7<sup>+</sup> N02 neutrophils through the receptors IL-1R2 and CXCR2 respectively, suggesting that the cellular hub of M01 macrophages and N02 neutrophils might be an important source of inflammation and immune injury in the lung (Figure 5A, B). We discovered that the BAFF (*TNFSF13B*), another ISG, expressed by IFN-responsive CXCL10<sup>+</sup> M06 macrophages, communicated with the follicular B cell maturation antigen BCMA (*TNFRSF17*), thus might promote the survival and activation of plasmablasts and plasma cells (Figure 5C). Besides, we also noticed that these M06 macrophages emanated signals to CD4<sup>+</sup>/PDCD1<sup>+</sup>/LAG3<sup>+</sup>T cells, CD8<sup>+</sup>/CD27<sup>+</sup> T cells and CD8<sup>+</sup>/KI67<sup>+</sup> T cells through the CXCL10-CXCR3 pair to induce their migration (Figure 5B, D). For neutrophils, we found that IFN-responsive ISG15<sup>+</sup> N03 neutrophils exhibited an elevated PD-L1 signal to interact with the PD-1 on CD4<sup>+</sup>/PDCD1<sup>+</sup>/LAG3<sup>+</sup>T cells (Figure 5A-C), thus might induce their exhaustion. Altogether, these data indicate that the signals from CXCL10<sup>+</sup> macrophages to B cells and ISG15<sup>+</sup> neutrophils to CD4<sup>+</sup> T cells respectively may help to eliminate viral infection and alleviate immune overactivation.

### 3.6 The comparison of cell components between Omicron and pre-Alpha/Alpha subvariants in single-cell transcriptional profiles

We performed viral metatranscriptome sequencing on lavage supernatant of all donors to explore the sub-lineages of the variant of concern Omicron. All 17 individuals were affiliated with the BA. sublineages and its descendants (BA.5, BF7, XBB, BQ.1, CL.1) as per the Pango lineage criteria (Supporting Information: Table S9).<sup>44</sup> To cluster the immune cells in the lungs of SARS-CoV-2 patients comprehensively, we performed a meta-analysis based on the previous data of severe COVID-19 BALF scRNA-seq of five independent clinical centers (Hamberg, Berlin, Leuven, Guangzhou, Shenzhen) from January 2020 to November 2020 to elucidate the similarity and discrepancy between pre-Alpha/Alpha and Omicron subvariants.<sup>16-18,41,45</sup> The sequence assignment of SARS-CoV-2 were not performed in these studies, however, we deduced that the subvariants of these cases were pre-Alpha/Alpha according to the timeline of the pandemic waves. In these studies, 29 male and 10 female patients of severe pre-Alpha/Alpha were included, and they were subjected to mechanical ventilation like our Omicron cases. We integrated these pre-Alpha/Alpha scRNA-seq data together with our Omicron datasets, and 202,223 high-quality cells were visualized in UMAP (Figure 6A, Supporting Information: Table S10). Five major cell types were divided, including neutrophils (*CRF3R*, *G0S2*), macrophages (*LYZ*, *CD68*), T/NK cells (*CD2*, *CD3D*, *NKG7*, *KLRD1*), epithelial cells (*KRT19*), B cells and plasma cells (*CD79A*, *MS4A1*, *MZB1*), the same as our Omicron datasets (Figure 6A, B). Neutrophils and macrophages still ranked the first and second in terms of their abundance (Supporting Information: Table S10).

The neutrophils and macrophages in the integrated datasets were then analyzed, and integration analysis redefined six subclusters of neutrophils and seven subclusters of macrophages (Figure 6C). For neutrophils, the Sankey data flow revealed that the signature data of merged N01 almost converged on Omicron N01 with marker genes *PI3*, *CCL3*, *CCL4L2*, and *SLAMF7*. Merged N02 mostly channeled into Omicron N02 with marker genes *CST7*, *S100A8* and *S100A9*. Merged N05 mostly channeled into Omicron N05 with marker genes *HSPA1A*, *HSPB1* and *DNAJB1*. Merged N06 was apt to Omicron N04 with marker genes *MMP8*, *MMP9* and *RETN*. Especially, the data flow of merged N04 exclusively channeled toward our Omicron N03, and they expressed similar marker genes such as *IFIT1* /2 /3 and *ISG15* (Figure 6D, E). Hence, merged N01 cells were similar to the inflammation-promotive PI3<sup>+</sup> neutrophils, merged N02 were the CST7<sup>+</sup> neutrophils, merged N04 cells were the ISG15<sup>+</sup> IFN-responsive neutrophils, merged N05 cells were the DNAJB1<sup>+</sup> stress-induced neutrophils, and merged N06 cells were similar to MMP9<sup>+</sup> immunosuppressive neutrophils.

For macrophages, we found some turbulence that post-integrated seven new subclusters exhibited a disordered mapping onto our primary seven Omicron cell subclusters. We speculated that this discrepancy might be ascribed to the fact that macrophage quantities in merged dataset were much more than those in Omicron group (42,220 vs. 14,644) (Figure 6D, Supporting Information: Table S10). We did not observe a separate IFN-responsive macrophage subset. However, merged M01 subset occupied over 50% of all macrophages, which expressed abounding pro-inflammatory cytokines like CCL3, CXCL2 and IL-1 $\beta$ , representing the pro-inflammatory CXCL5<sup>+</sup> M01 and VCAN<sup>+</sup> M03 macrophages in Omicron dataset. Besides, merged M02 and M03 exhibited high expression of *C1QA*, *C1QB*, *C1QC*, *APOC1*, *APOE* and *FABP4*, indicative of alveolar/interstitial macrophages (Figure 6D, E).

We found that PI3<sup>+</sup> N01 neutrophils were significantly higher in pre-Alpha/Alpha group, and MMP9<sup>+</sup> N06 neutrophils were significantly higher in Omicron group. Although the median of CST7<sup>+</sup> N02 neutrophils and ISG15<sup>+</sup> N03 neutrophils seemed to be increased in Omicron subvariants, we failed to reject the null hypothesis. For macrophages, merged pro-inflammatory M01 macrophages were more abundant in Omicron, and merged APOC1<sup>+</sup>/APOE<sup>+</sup>/FABP4<sup>+</sup>M02 macrophages, possessing phagocytosis and damage repair function, were more abundant in pre-Alpha/Alpha group (Figure 6F). The comparison of neutrophil and macrophage subsets in severe pre-Alpha/Alpha and Omicron cases suggested that the alveolar inflammation of these subvariants might be mediated by different cell components. In pre-Alpha/Alpha variant, inflammation-promotive PI3<sup>+</sup>merged N01 neutrophils are more, while damage repair APOC1<sup>+</sup>/APOE<sup>+</sup>/FABP4<sup>+</sup>merged M02 macrophages are more. On the contrary, in Omicron variant, inflammation-promotive IL-1 $\beta$ <sup>+</sup>/CXCL<sup>+</sup>merged M01 macrophages are more, while immunosuppressive MMP9<sup>+</sup> merged N06 neutrophils are more. These explanations indicate that the underlying cellular remodeling for the development of severe disease may be different between pre-Alpha/Alpha and Omicron variants, which may be conducive to the future guidance for the clinical practice against severe Omicron diseases.

#### 4. DISCUSSION

One of the hallmarks in senile patients of severe COVID-19 is the hypoxemia, which frequently deteriorates into ARDS, with the cytokine storm in both the systemic circulation and the pulmonary tissue.<sup>46</sup> Another horrible issue is the hospital-acquired infections, and the bacterial co-infections always bring about a tough challenge in ICU.<sup>47-49</sup> The mortality of Omicron severe patients is often attributed to sepsis-induced ARDS and multi-organ failure, which is similar in the severe pre-Alpha/Alpha cases.<sup>20</sup> Studies suggested that the SOFA score had a discriminative capacity to tell the adverse outcome from the critical-ill patients with COVID-19 sepsis.<sup>50</sup> In the meantime, CPIS holds a positive correlation between the clinical severity and quantitative bacteriology of the pneumonia.<sup>51</sup> In our study, we provided a single-cell transcriptome atlas to generate the cellular profiles and cell-cell interactions in the lung of lethal Omicron, which linked the levels of the IFN-responsive neutrophils and macrophages with low CPIS grades, and the pro-inflammatory or septic neutrophils and macrophages with worse SOFA scores, thus suggesting the potential biomarkers for the identification of disease severity and the underlying functions of these cell subsets in the progression of severe Omicron.

The inflammation and infiltration of myeloid cells including neutrophils and macrophages in the lung were discovered by our study to be the predominant characteristic of severe Omicron, which is similar to that of critical pre-Alpha/Alpha. The intense inflammatory environment in the alveoli was mediated by these myeloid cells, especially PI3<sup>+</sup> neutrophils, CST7<sup>+</sup> neutrophils, VCAN<sup>+</sup> macrophages and CXCL5<sup>+</sup> macrophages, which produced large amounts of pro-inflammatory cytokines and chemokines, thus promoting the progression of alveolar inflammation. The CST7<sup>+</sup> neutrophils and VCAN<sup>+</sup> macrophages were positively correlated with SOFA grades, while CXCL5<sup>+</sup> macrophages were positively correlated with CPIS grades, further demonstrating their important roles in the development of excessive alveolar inflammation. In contrast, lymphoid-derived cells accounted for a minor inflammatory proportion. Thus, the control of the overactivated myeloid inflammatory cells is still the main direction to intervene the progression of severe Omicron pneumonia.

The beneficial cell subsets also existed in the alveolar milieu of critical Omicron, which was suggested to indicate lower lung infection. ISG15<sup>+</sup> neutrophils and CXCL10<sup>+</sup> macrophages, both demonstrated to be IFN-responsive, were determined to be negatively correlated with the CPIS grades of severe Omicron patients. However, these two cell subsets have not been excavated or reported in the previous scRNA-seq studies of COVID-19, suggesting they may be Omicron-specific cell subpopulations. In the pseudotime analysis of these two ISG15<sup>+</sup> neutrophils and CXCL10<sup>+</sup> macrophages, they maintained a constant number throughout the differentiation and development trajectory. Nevertheless, their expression of ISGs peaked at the mid-to-late stages of the lineage evolution. We presumed that, if the production of host IFN emerged earlier and stronger, these two cell subsets may be enhanced, and their expression of ISGs and the favorable biological functions may be strengthened. Thus, the treatment with IFN, especially in the early phase of Omicron infection, may be useful to the prevention of severe pneumonia and the intervention of critical ARDS. Previously, clinical treatments against critical COVID-19 largely honed in on alleviating the overactivated alveolar inflammation and cytokine storm, such as using the tocilizumab to neutralize pro-inflammatory IL-6.<sup>52</sup> Together with the present study, the combination of anti-inflammatory agents with IFN may be beneficial in the treatment of severe Omicron pneumonia.

For the potential biological functions of the beneficial ISG15<sup>+</sup> neutrophils and CXCL10<sup>+</sup> macrophages, we discovered that ISG15<sup>+</sup> neutrophils were positively correlated with the protective alveolar epithelial cells, which might help the rejuvenation of the epithelial barrier. Moreover, ISG15<sup>+</sup> neutrophils also expressed PD-L1, which may attenuate the hyperactivated T cells-mediated immune injury through the PD-L1-PD1 axis. Meanwhile, CXCL10<sup>+</sup> macrophages might activate B cell-mediated humoral immunity through the BAFF signal, indicating the potential preventative antiviral humoral immune response. However, all these deductions still need further validation in the study of SARS-CoV-2 mouse models in vivo.

For the alveolar cell subsets in severe Omicron and previous pre-Alpha/Alpha, our scRNA-seq analysis of BALF did not find the existence of dendritic cells, such as pDC, cDC1, cDC2, which were determined to be present in the BALF of severe pre-Alpha/Alpha and were plentiful in the BALF and PBMCs of mild COVID-19 cases.<sup>18,53</sup> In the context of severe Omicron infection, we have identified IFN-responsive ISG15<sup>+</sup> neutrophils as a separate cellular subset, an identification not previously established in the analysis of severe cases of pre-Alpha/Alpha variants. Instead, these neutrophils in severe pre-Alpha/Alpha expressing ISGs in conjunction with *CSF3R*, *S100A8* and *S100A9*, which exhibited a dual expression profile, encompassing both ISGs and genes associated with pro-inflammatory responses.<sup>29</sup> However, in severe Omicron here, these neutrophils are two separate cell subsets, septic CST7<sup>+</sup> neutrophils and ISG15<sup>+</sup> neutrophils. These two cell subsets may possess opposite functions, one is pro-inflammatory while the other may be protective and correlated with alleviated phenotypes. These differences may represent the unique characteristics of severe Omicron as compared to the previous variants.

Although our BALF immune landscape suggested the potential roles of neutrophils and macrophages in the progression of severe Omicron infection, our study has several limitations, including the stochastic and limited patients without pre-stratification, no comparative severe cases caused by the infection of bacterial solely or other virus, no control BALF from healthy donors or convalescents because of the ethical reasons, and no comparative study with the BALF from the Omicron mild cases.

In summary, we provided a BALF single-cell atlas of critical Omicron patients, and suggests the immune landscape, especially neutrophils and macrophages, in the lung of severe cases. The alveolar IFN-responsive ISG15<sup>+</sup> neutrophils and CXCL10<sup>+</sup> macrophages are negatively correlated with disease severity, and these two cell subsets may extricate Omicron critical patients from the nasty fate of sepsis.

## AUTHOR CONTRIBUTIONS

All authors meet authorship requirements. Mu Wang, Dingji Zhang, Ting Lei, Ye Zhou, and Hao Qin performed the experiments and contributed equally to the whole study. Yuchao Dong, Wei Zhang, and Hao Qin provided human samples. Yanfeng Wu, Shuxun Liu, Liyuan Zhang, Kaiwei Jia, Yue Dong, Suyuan Wang, Yunhui Li, Yiwen Fan, and Liangchen Gui provided reagents. Zhixuan Li and Mu Wang performed the data analysis. Mu Wang drafted the original manuscript. Jin Hou supervised the study and revised the paper. All authors have read and approved the final manuscript.

## ACKNOWLEDGEMENTS

We thank Ms. Tingting Fang from our laboratory for the technical assistance. This work was supported by grants from the National Natural Science Foundation of China (92269204, 92369106, 82171755, 82171749, 82071796), the Military Outstanding Youth Program (23SWAQ53, 01-SWKJYCJJ07, 2020QN06119), and the Emergency Key Program of Guangzhou Laboratory (EKPG21-30-3).

## CONFLICT OF INTEREST

The authors declare no competing interest.

## DATA AVAILABILITY STATEMENT

The single-cell gene expression matrices and integrated objects are accessible through the Gene Expression Omnibus under GSE263469. The viral metatranscriptome was uploaded at the public Sequence Read Archive (SRA) under RPJNA1091557.

## ETHICS STATEMENT

The Ethics Committee approval was obtained from the Research Ethics Committee of the First Affiliated Hospital of Second Military Medical University, Shanghai. All patients included in this study provided written informed consent.

## ORCID

*Jin Hou* 0000-0002-8670-517X

## REFERENCES

1. Dhama K, Nainu F, Frediansyah A, et al. Global emerging Omicron variant of SARS-CoV-2: impacts, challenges and strategies. *J Infect Public Health* . 2023;16(1):4-14.
2. Sokal A, Barba-Spaeth G, Hunault L, et al. SARS-CoV-2 Omicron BA.1 breakthrough infection drives late remodeling of the memory B cell repertoire in vaccinated individuals. *Immunity* . 2023;56(9):2137-2151.
3. Altmann DM, Boyton RJ. Arming up against Omicron subvariants. *Cell Host Microbe* . 2024;32(2):147-148.
4. Esper FP, Adhikari TM, Tu ZJ, et al. Alpha to Omicron: disease severity and clinical outcomes of major SARS-CoV-2 variants. *J Infect Dis* . 2023;227(3):344-352.
5. Kim T, Min KI, Yang JS, et al. Relative infectivity of the SARS-CoV-2 Omicron variant in human alveolar cells. *iScience* . 2022;25(12):105571.
6. Arabi M, Al-Najjar Y, Mhaimed N, et al. Severity of the Omicron SARS-CoV-2 variant compared with the previous lineages: a systematic review. *J Cell Mol Med* . 2023;27(11):1443-1464.

7. Ren X, Wen W, Fan X, et al. COVID-19 immune features revealed by a large-scale single-cell transcriptome atlas. *Cell* . 2021;184(7):1895-1913.
8. Schulte-Schrepping J, Reusch N, Paclik D, et al. Severe COVID-19 is marked by a dysregulated myeloid cell compartment. *Cell* . 2020;182(6):1419-1440.
9. Wilk AJ, Rustagi A, Zhao NQ, et al. A single-cell atlas of the peripheral immune response in patients with severe COVID-19. *Nat Med* . 2020;26(7):1070-1076.
10. Stephenson E, Reynolds G, Botting RA, et al. Single-cell multi-omics analysis of the immune response in COVID-19. *Nat Med* . 2021;27(5):904-916.
11. COvid-19 Multi-omics Blood Atlas (COMBAT) Consortium. A blood atlas of COVID-19 defines hallmarks of disease severity and specificity. *Cell* . 2022;185(5):916-938.
12. Unterman A, Sumida TS, Nouri N, et al. Single-cell multi-omics reveals dyssynchrony of the innate and adaptive immune system in progressive COVID-19. *Nat Commun* . 2022;13(1):440.
13. Zhang JY, Wang XM, Xing X, et al. Single-cell landscape of immunological responses in patients with COVID-19. *Nat Immunol* . 2020;21(9):1107-1118.
14. Xu G, Qi F, Wang H, et al. The transient IFN response and the delay of adaptive immunity feature the severity of COVID-19. *Front Immunol* . 2021;12:816745.
15. Zhang F, Mears JR, Shakib L, et al. IFN-gamma and TNF-alpha drive a CXCL10<sup>+</sup> CCL2<sup>+</sup> macrophage phenotype expanded in severe COVID-19 lungs and inflammatory diseases with tissue inflammation. *Genome Med* . 2021;13(1):64.
16. Liao M, Liu Y, Yuan J, et al. Single-cell landscape of bronchoalveolar immune cells in patients with COVID-19. *Nat Med* . 2020;26(6):842-844.
17. Chua RL, Lukassen S, Trump S, et al. COVID-19 severity correlates with airway epithelium-immune cell interactions identified by single-cell analysis. *Nat Biotechnol* . 2020;38(8):970-979.
18. Wauters E, Van Mol P, Garg AD, et al. Discriminating mild from critical COVID-19 by innate and adaptive immune single-cell profiling of bronchoalveolar lavages. *Cell Res* . 2021;31(3):272-290.
19. Bost P, Giladi A, Liu Y, Bendjelal Y, Xu G, David E, et al. Host-viral infection maps reveal signatures of severe COVID-19 patients. *Cell* . 2020;181(7):1475-1488.
20. Wai AKC, Lee TTL, Chan SCL, et al. Association of molnupiravir and nirmatrelvir-ritonavir with reduced mortality and sepsis in hospitalized omicron patients: a territory-wide study. *Sci Rep* . 2023;13(1):7832.
21. Imbiakha B, Ezzatpour S, Buchholz DW, et al. Age-dependent acquisition of pathogenicity by SARS-CoV-2 Omicron BA.5. *Sci Adv* . 2023;9(38):eadj1736.
22. de Prost N, Audureau E, Heming N, et al. Clinical phenotypes and outcomes associated with SARS-CoV-2 variant Omicron in critically ill French patients with COVID-19. *Nat Commun* . 2022;13(1):6025.
23. Dura B, Choi JY, Zhang K, et al. scFTD-seq: freeze-thaw lysis based, portable approach toward highly distributed single-cell 3' mRNA profiling. *Nucleic Acids Res* . 2019;47(3):e16.
24. Alwani M, Yassin A, Al-Zoubi RM, et al. Sex-based differences in severity and mortality in COVID-19. *Rev Med Virol* . 2021;31(6):e2223.
25. Traish AM. Sex steroids and COVID-19 mortality in women. *Trends Endocrinol Metab* . 2021;32(8):533-536.

26. Shankar-Hari M, Phillips GS, Levy ML, et al. Developing a new definition and assessing new clinical criteria for septic shock: for the third international consensus definitions for sepsis and septic shock (sepsis-3). *JAMA* . 2016;315(8):775-787.
27. Silvin A, Chapuis N, Dunsmore G, et al. Elevated calprotectin and abnormal myeloid cell subsets discriminate severe from mild COVID-19. *Cell* . 2020;182(6):1401-1418.
28. Yao RQ, Zhao PY, Li ZX, et al. Single-cell transcriptome profiling of sepsis identifies HLA-DRlowS100Ahigh monocytes with immunosuppressive function. *Mil Med Res* . 2023;10(1):27.
29. Sinha S, Rosin NL, Arora R, et al. Dexamethasone modulates immature neutrophils and interferon programming in severe COVID-19. *Nat Med* . 2022;28(1):201-211.
30. Schultze JL, Mass E, Schlitzer A. Emerging principles in myelopoiesis at homeostasis and during infection and inflammation. *Immunity*. 2019;50(2):288-301.
31. Li Z, Chen X, Dan J, et al. Innate immune imprints in SARS-CoV-2 Omicron variant infection convalescents. *Signal Transduct Target Ther* . 2022;7(1):377.
32. Delorey TM, Ziegler CGK, Heimberg G, et al. COVID-19 tissue atlases reveal SARS-CoV-2 pathology and cellular targets. *Nature* . 2021;595(7865):107-113.
33. Cui Z, Zeng C, Huang F, Yuan F, Yan J, Zhao Y, et al. Cas13d knockdown of lung protease Ctsl prevents and treats SARS-CoV-2 infection. *Nat Chem Biol* . 2022;18(10):1056-1064.
34. Upadhyay AA, Viox EG, Hoang TN, Boddapati AK, Pino M, Lee M Y-H, et al. TREM2<sup>+</sup> and interstitial-like macrophages orchestrate airway inflammation in SARS-CoV-2 infection in rhesus macaques. *Nat Commun* . 2023;14(1):1914.
35. Zhang B, Zhang Y, Xiong L, et al. CD127 imprints functional heterogeneity to diversify monocyte responses in inflammatory diseases. *J Exp Med* . 2022;219(2):e20211191.
36. Björklund ÅK, Forkel M, Picelli S, et al. The heterogeneity of human CD127<sup>+</sup> innate lymphoid cells revealed by single-cell RNA sequencing. *Nat Immunol*. 2016;17(4):451-460.
37. Tian Y, Carpp LN, Miller HER, et al. Single-cell immunology of SARS-CoV-2 infection. *Nat Biotechnol* . 2022;40(1):30-41.
38. Karmaus PWF, Tata A, Meacham JM, et al. Meta-analysis of COVID-19 BAL single-cell RNA sequencing reveals alveolar epithelial transitions and unique alveolar epithelial cell fates. *Am J Respir Cell Mol Biol* . 2023;69(6):623-637.
39. Kobayashi Y, Tata A, Konkimalla A, et al. Persistence of a regeneration-associated, transitional alveolar epithelial cell state in pulmonary fibrosis. *Nat Cell Biol* . 2020;22(8):934-946.
40. Choi J, Park JE, Tsagkogeorga G, et al. Inflammatory signals induce AT2 cell-derived damage-associated transient progenitors that mediate alveolar regeneration. *Cell Stem Cell* . 2020;27(3):366-382.
41. He J, Cai S, Feng H, et al. Single-cell analysis reveals bronchoalveolar epithelial dysfunction in COVID-19 patients. *Protein Cell* . 2020;11(9):680-687.
42. Reyfman PA, Walter JM, Joshi N, et al. Single-cell transcriptomic analysis of human lung provides insights into the pathobiology of pulmonary fibrosis. *Am J Respir Crit Care Med* . 2019;199(12):1517-1536.
43. Lin Y, Qi Y, Jiang M, et al. Lactic acid-induced M2-like macrophages facilitate tumor cell migration and invasion via the GPNMB/CD44 axis in oral squamous cell carcinoma. *Int Immunopharmacol* . 2023;124(Pt B):110972.
44. O'Toole Á, Pybus OG, Abram ME, et al. Pango lineage designation and assignment using SARS-CoV-2 spike gene nucleotide sequences. *BMC Genomics* . 2022;23(1):121.

45. Zhao Y, Kilian C, Turner JE, et al. Clonal expansion and activation of tissue-resident memory-like Th17 cells expressing GM-CSF in the lungs of severe COVID-19 patients. *Sci Immunol* . 2021;6(56):eabf6692.
46. Del Valle DM, Kim-Schulze S, Huang HH, et al. An inflammatory cytokine signature predicts COVID-19 severity and survival. *Nat Med* . 2020;26(10):1636-1643.
47. Alessandri F, d’Ettorre G, Ciccozzi M, et al. Early recognition of a superinfection: this is the problem in the critically ill COVID-19 patients. *J Med Virol* . 2024;96(1):e29345.
48. Parczewski M, Kuffel J, Aksak-Was B, et al. Artificial neural network based prediction of the lung tissue involvement as an independent in-hospital mortality and mechanical ventilation risk factor in COVID-19. *J Med Virol* . 2023;95(5):e28787.
49. De Francesco MA, Signorini L, Piva S, et al. Bacterial and fungal superinfections are detected at higher frequency in critically ill patients affected by SARS CoV-2 infection than negative patients and are associated to a worse outcome. *J Med Virol* . 2023;95(7):e28892.
50. Moisa E, Corneci D, Negutu MI, et al. Development and internal validation of a new prognostic model powered to predict 28-day all-cause mortality in ICU COVID-19 patients-the COVID-SOFA score. *J Clin Med* . 2022;11(14):4160.
51. Zilberberg MD, Shorr AF. Ventilator-associated pneumonia: the clinical pulmonary infection score as a surrogate for diagnostics and outcome. *Clin Infect Dis* . 2010;1:51,Suppl 1:S131-135.
52. Qin G, Liu S, Yang L, et al. Myeloid cells in COVID-19 microenvironment. *Signal Transduct Target Ther* . 2021;6(1):372.
53. Saichi M, Ladjemi MZ, Korniotis S, et al. Single-cell RNA sequencing of blood antigen-presenting cells in severe COVID-19 reveals multi-process defects in antiviral immunity. *Nat Cell Biol* . 2021;23(5):538-551.

Figure 1

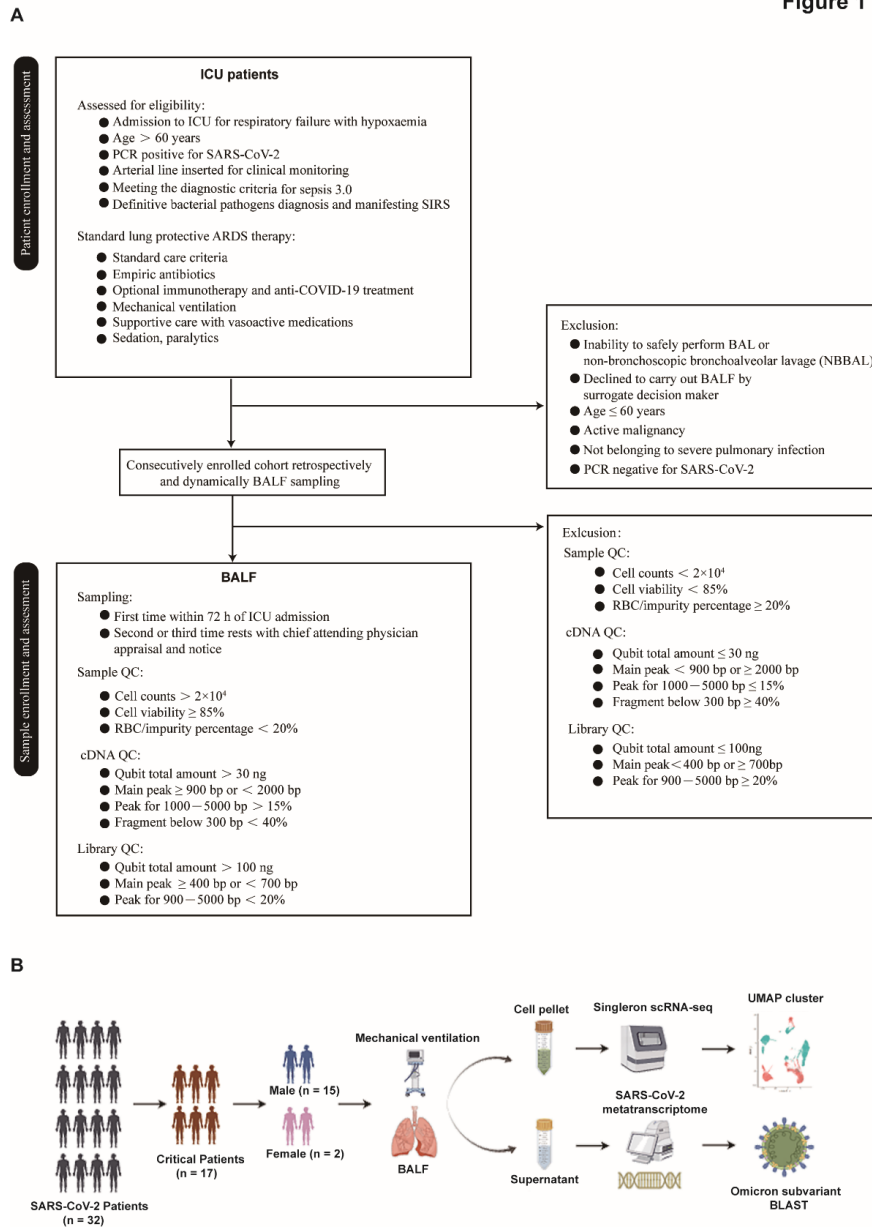


**FIGURE 1 Overview of study design and sampling procedure**

(A) An evaluated process regarding sample eligibility.

(B) Sample cohort, viral metatranscriptomic sequencing of BALF supernatant and single-cell sequencing sampling procedure of cellular precipitate.

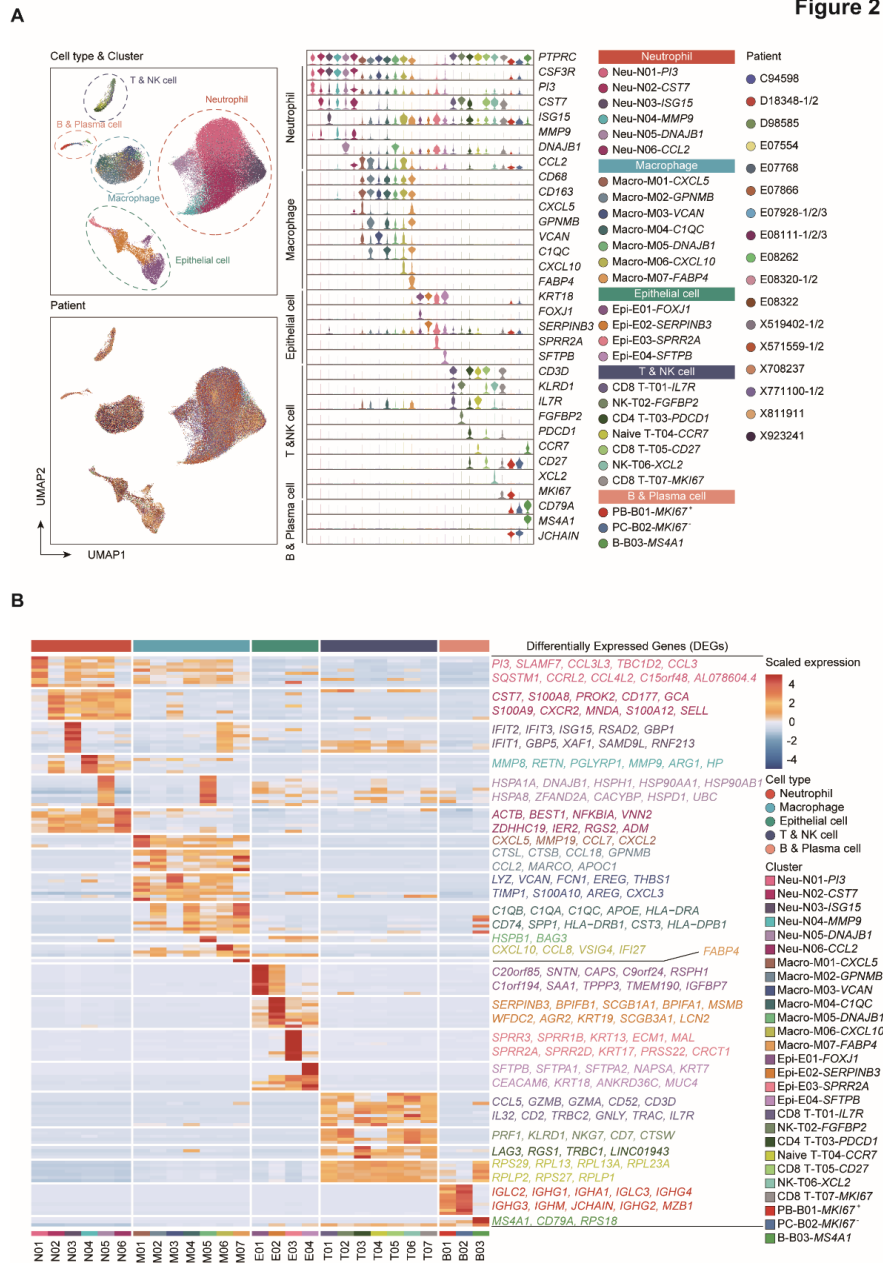


**FIGURE 2. Bronchoalveolar single-cell profile signature in BALF from critical Omicron patients**

(A) UMAP projection embedding of cross-sample batch-corrected PCA matrix. The entire dataset from the whole 112,926 cells colored by orthogonally inferred cell identity labelled by automated cell type annotation (left). Stacked violin plot showing the scaled expression of optimal signature genes (rows) and the subclusters of the manual post hoc annotations (columns) with the same color as the names to the right (middle). All profiled samples from 17 Omicron patients and sample IDs beginning with “C, D, E, X” with different color shade (right).

(B) Heatmap of top marker genes for 27 identified cell types with scaled expression. All displayed genes are

statistically significant at the  $p < 0.05$  confidence. Genes defined as positive for a cell if at least one UMI of that gene was found.

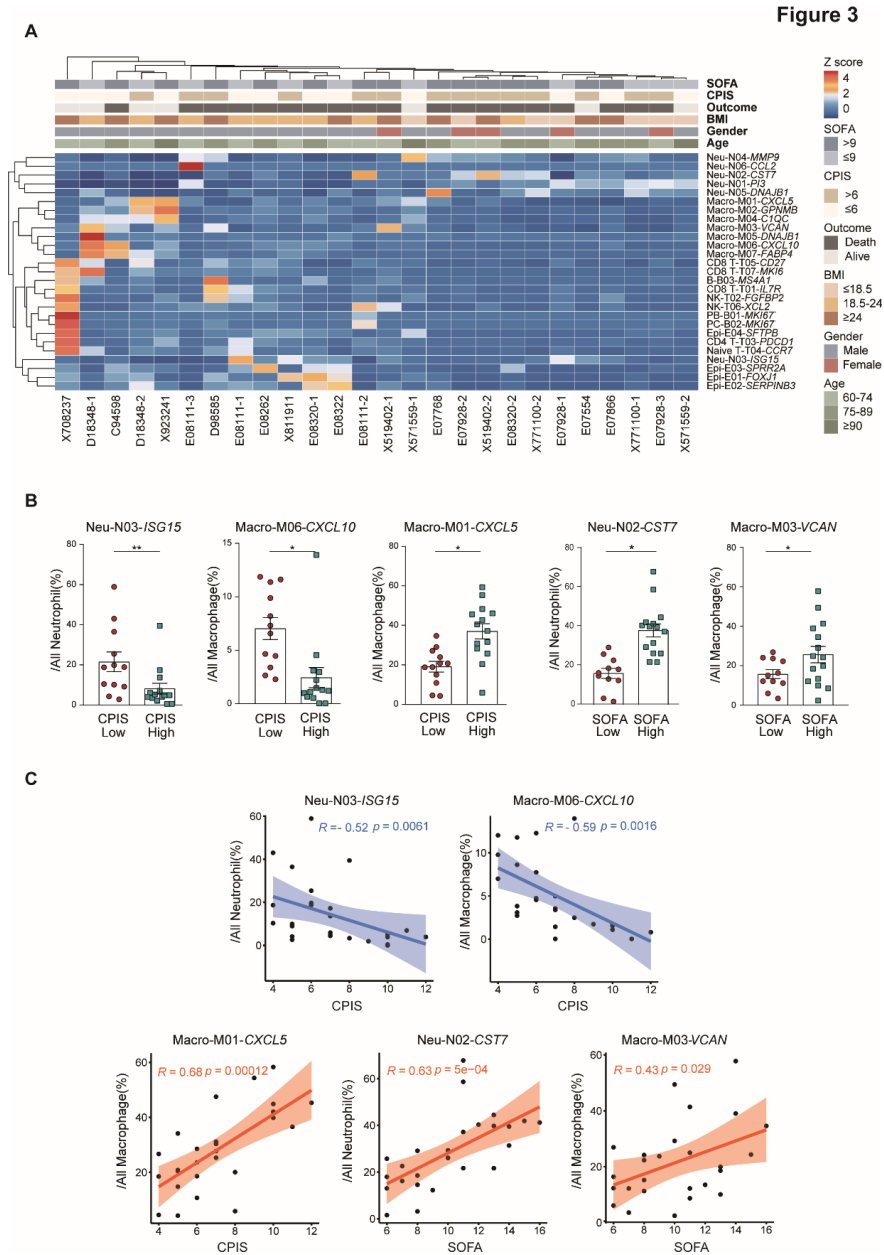


**FIGURE 3. Alveolar neutrophils and macrophages correlated with CPIS and SOFA grades in severe Omicron patients**

(A) Heatmap visualizing the Z-score of the relative abundance using hierarchical Ward's D2 linkage clustering based on Euclidean distances (scaled in row). Each row representing a subcluster ( $n=27$ ) and each column representing a sample ( $n=26$ ).

(B) Bar plots showing the percentage of N03, M06 and M01 of the main cell types in each sample grouped by CPIS, the percentage of N02 and M03 of the main cell types in each sample grouped by SOFA. Significance

was estimated using two-tailed Mann-Whitney U test. The results presented as means  $\pm$  S.E.M.; \* $p < 0.05$ , \*\* $p < 0.01$ .

(C) Scatter plots depicting the correlation between the percentage of N03, M06, M01 and CPIS, the correlation between the percentage of N02, M03 and SOFA. The coefficient “ $R$ ” of Spearman correlation representing the strength of correlation and  $p$  values shown for each comparison.

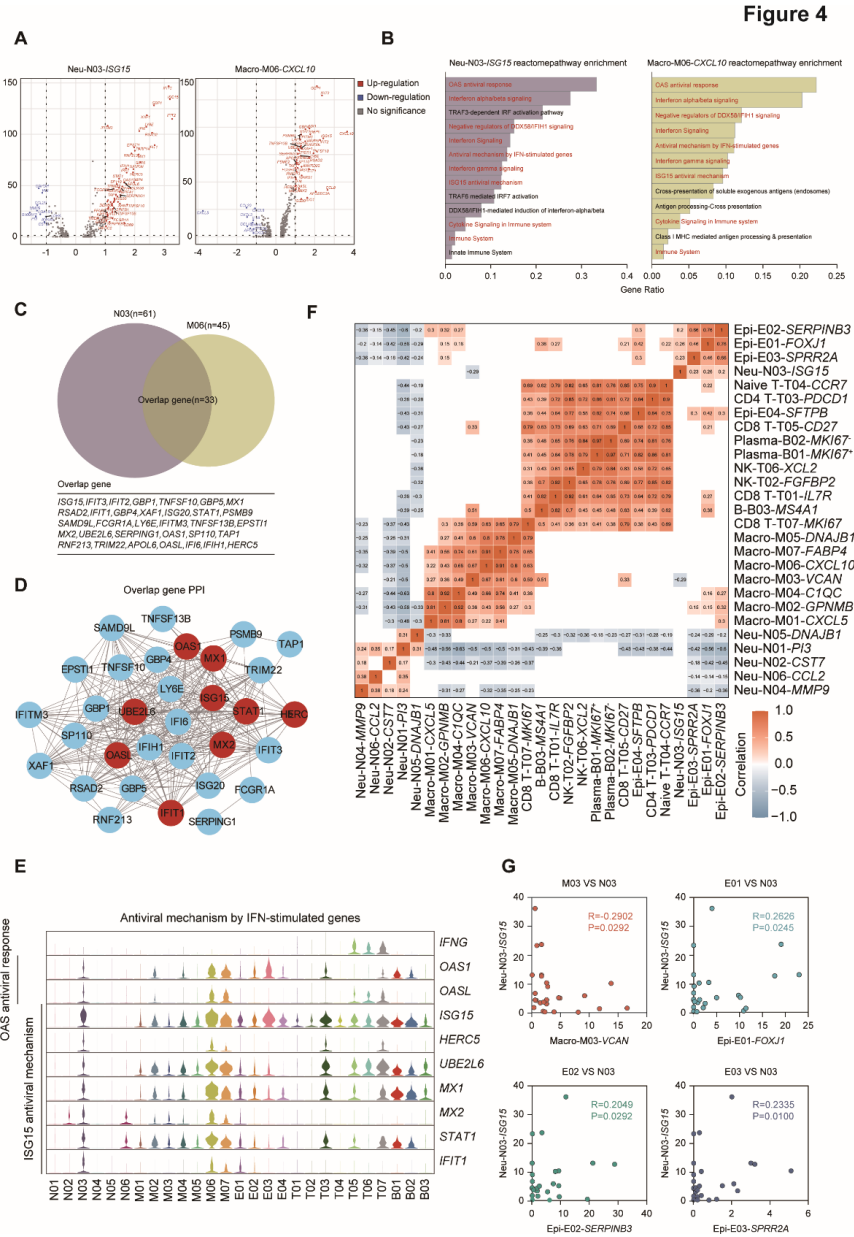


**FIGURE 4. The correlation of ISG15<sup>+</sup> neutrophils and CXCL10<sup>+</sup> macrophages with other cell subsets in the BALF from severe Omicron patients**

(A) Volcano plot for significance  $[-\log_{10} (p \text{ value})$ , Y-axis] versus magnitude  $[\log_2 (\text{fold change})$ , X-axis] of specific differential expression of each gene (dots; horizontal dashed line,  $\text{FDR} < 0.05$ ; vertical dashed lines, |

$\log_2(\text{fold change}) = 1$  in N03 and M06 subclusters. Each subcluster versus all other subclusters as control in the same major cluster. Upregulation colored in red; downregulation colored in blue; no significance colored in gray.

(B) Signaling pathways enriched in N03 and M06 relative to remaining cells in the same major cluster using Reactome database. Enrichment pathways depicting top positively regulated terms.

(C) Differentially upregulated consensus genes of N03 (left, n=61) and M06 (right, n=45) in the Venn modality (middle, n=33).

(D) Protein-protein interaction (PPI) network of overlapped ISGs; pivotal nodes in red and fringe nodes in blue. Edges in gray denoting the interaction as confidence score  $> 0.5$  presented.

(E) Stacked violin plot showing the expression levels of genes under the OAS and ISG15 antiviral pathways in different subclusters.

(F) Correlation matrix heatmap of Spearman correlation analysis among subcluster-to-subcluster. Correlation coefficients “ $R$ ” shown at the intersection of the considered two subclusters (positive correlation coefficients, shadows of red; negative correlation coefficients, shadows of blue, correlations not statistically significant, being left blank).

(G) Scatter plots depicting the correlation between M03 and N03, E01 and N03, E02 and N03, E03 and N03. Spearman correlation coefficient “ $R$ ” and p values shown for each comparison.

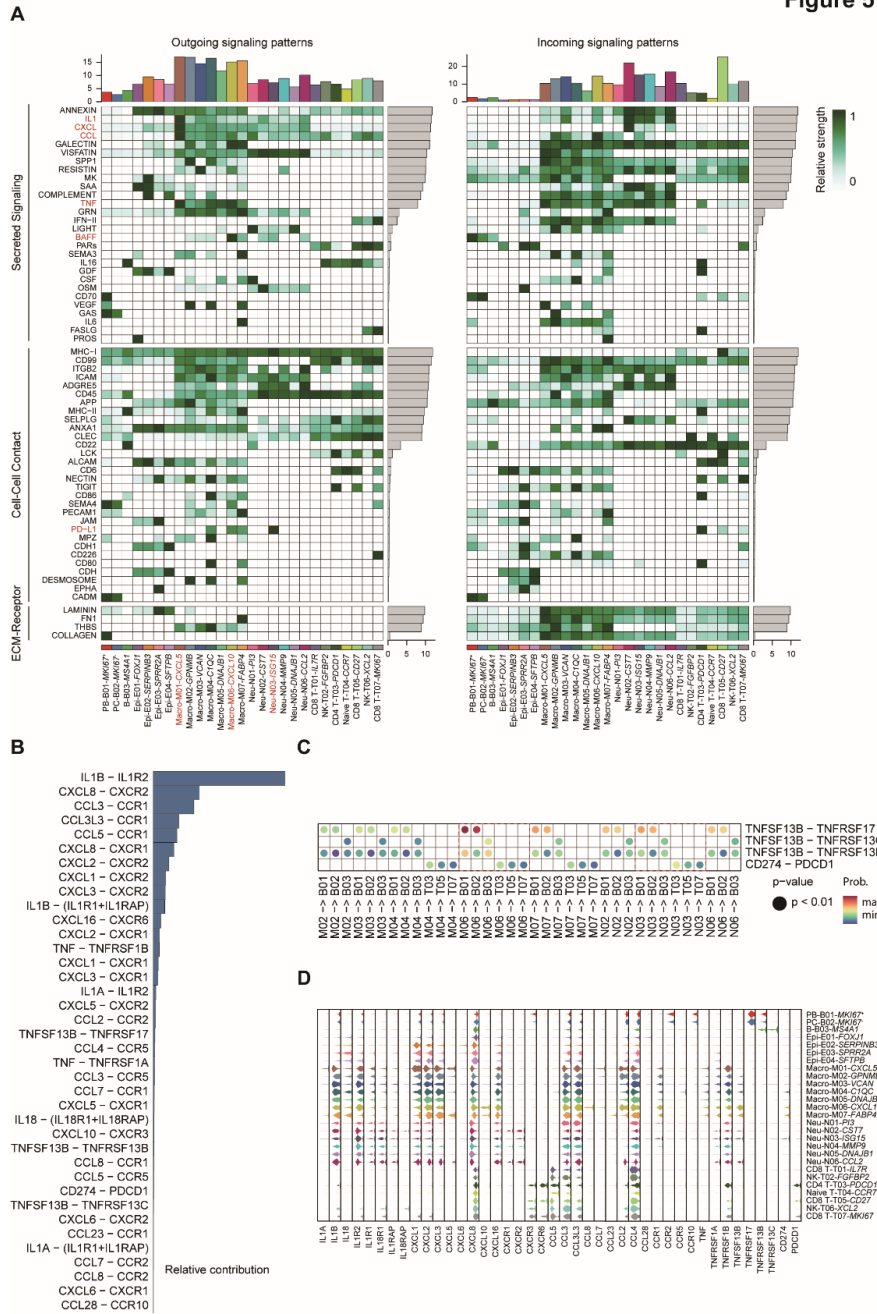


**FIGURE 5. Ligand-receptor interactions of CXCL5<sup>+</sup> macrophages, CXCL10<sup>+</sup> macrophages and ISG15<sup>+</sup> neutrophils**

(A) Interaction heatmap generalization of differential numbers of outgoing (left) and incoming (right) cell-to-cell interactions. Signaling strength with color-coded bars as per subclusters on the top and ligand-receptor interaction strength with gray bars as per signals on the right. Differentially relative strength bar of each signal by each subcluster laid out on the far right (white, low strength; green, high strength).

(B) Bar plot showing selected ligand-receptor pairs ranked as relative contribution value. Y-axis representing

individual ligand-receptor pairs while X-axis denoting the magnitude of their contribution.

(C) Differential enrichment of specific ligand-receptor interactions (rows) of macrophages and neutrophils with T cells and B cells/PBs/PCs (columns). Color-coded dots representing communication probability based on  $\log_2$  (fold change) of inferred ligand-receptor expression. Dot size depicting p value ( $p < 0.01$ ).

(D) Stacked violin plot showing the average expression of selected ligands or receptors for each subcluster.

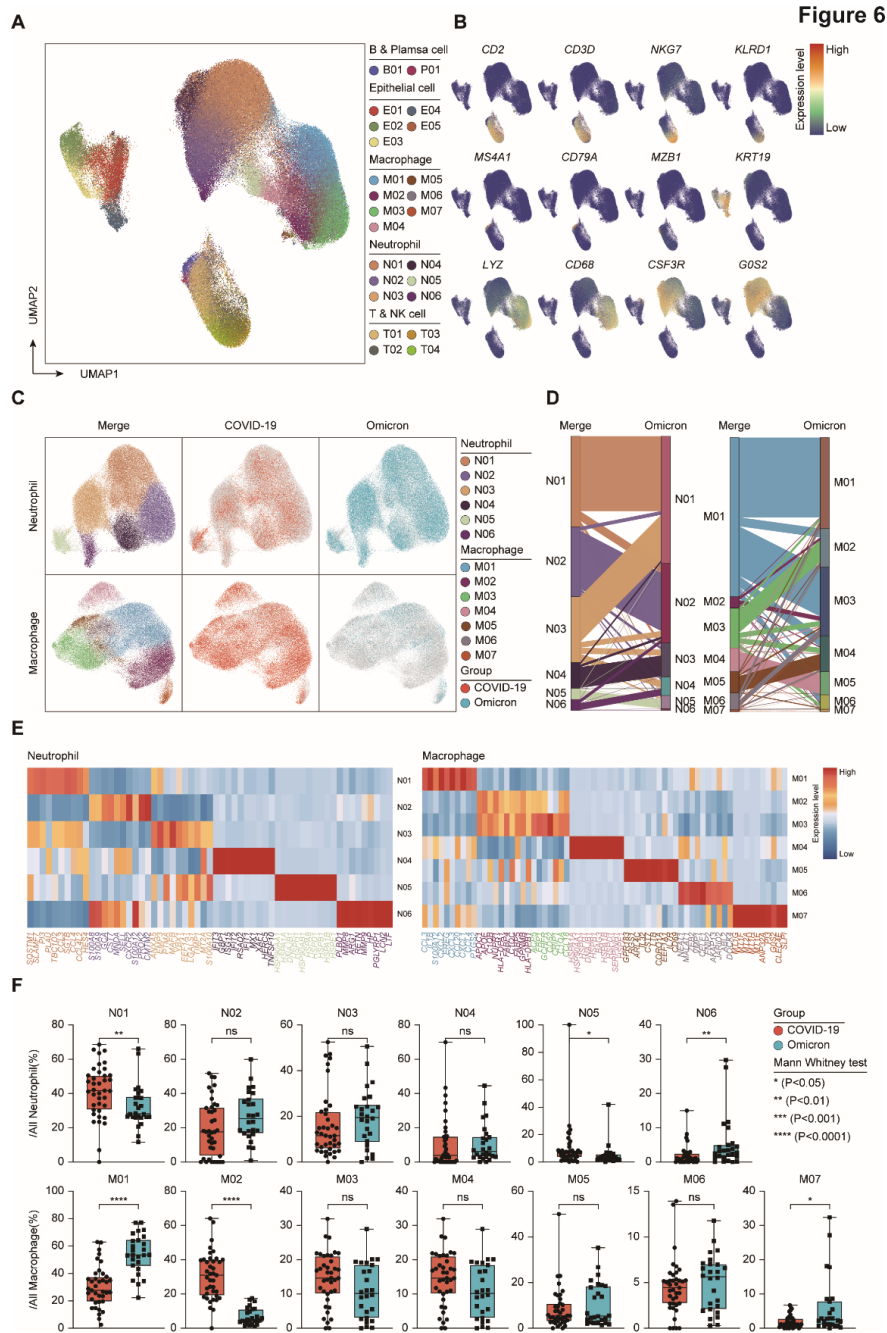


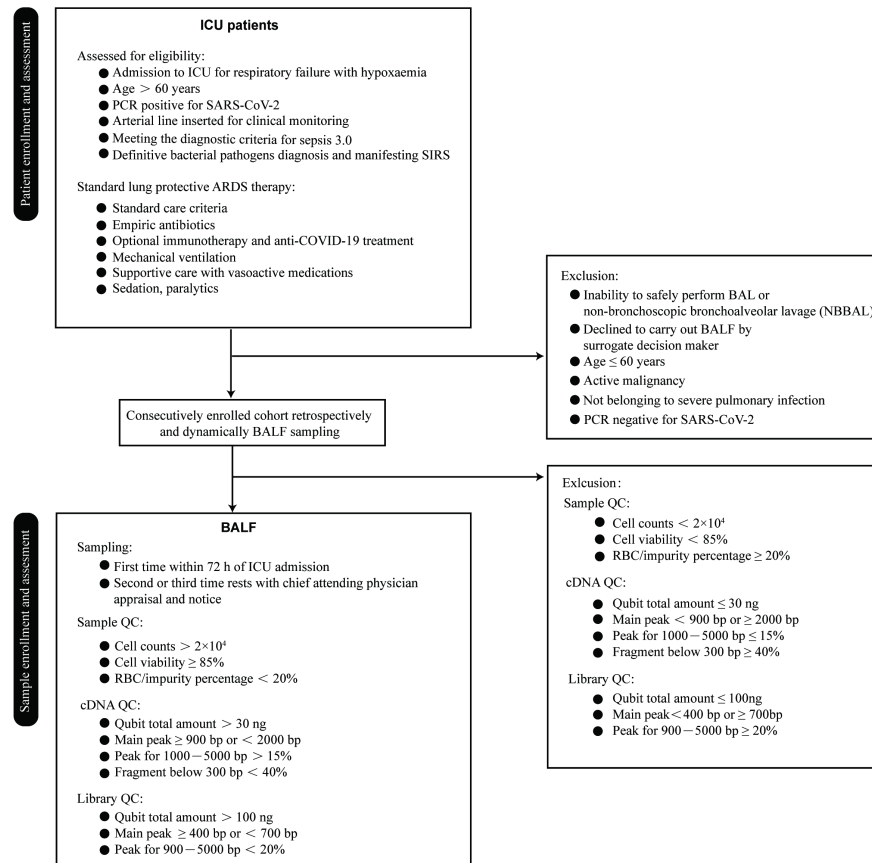
**FIGURE 6. ScRNA-seq data revealing the accordance and difference of cell composition**

## between severe Omicron and pre-Alpha/Alpha

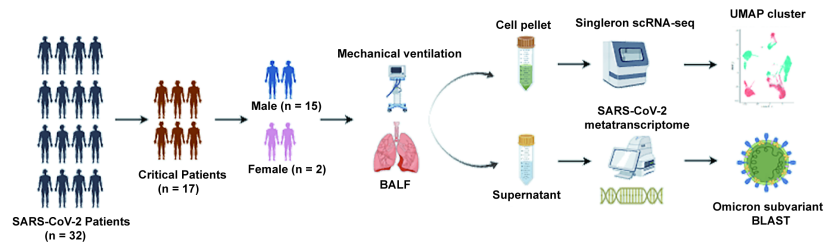
- (A) Cellular populations identified by UMAP projection of 202,223 single cells as Neutrophils (n=99,839), Macrophages (n=54,568), T/NK cells (n=25,151), Epithelial cells (n=20,253), B cells (n=1,682) and Plasma cells (n=730). Each dot corresponding to a single cell, colored according to major cell types with respective cell labels.
- (B) FeaturePlot of estimated density of merged marker genes overlay after batch correction showing distribution of separated subclusters. Color bar reflecting the expression levels.
- (C) UMAP embedding of myeloid subclusters after re-integration across pre-Alpha/Alpha (COVID-19) datasets and Omicron datasets. Cell subclusters in merged frame by manual curation with different colors.
- (D) Sankey diagram showing stacked subcluster proportion transforming. Each line representing a data flow from Merge to Omicron. The width of each line representing the size of the data flow.
- (E) Heatmap showing the Z-score normalized mean expression of selected top differentially expressed genes per subcluster. Color bar with the expression levels.
- (F) Fraction of myeloid subclusters in pre-Alpha/Alpha (n=39) and Omicron (n=26). Each dot corresponding to a single sample; \*p < 0.05, \*\*p < 0.01, \*\*\*p < 0.001, \*\*\*\*p < 0.0001; middle line, median; box edges, 25th and 75th percentiles; whiskers, most extreme points that do not exceed  $\pm 1.5 \times$  the interquartile range (IQR); two-tailed Mann-Whitney U test.

Figure 1

A



B



A

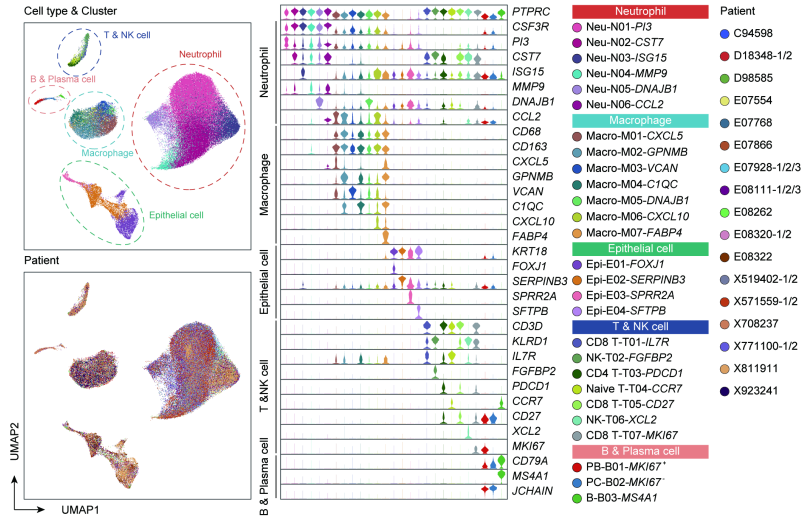


Figure 2

B

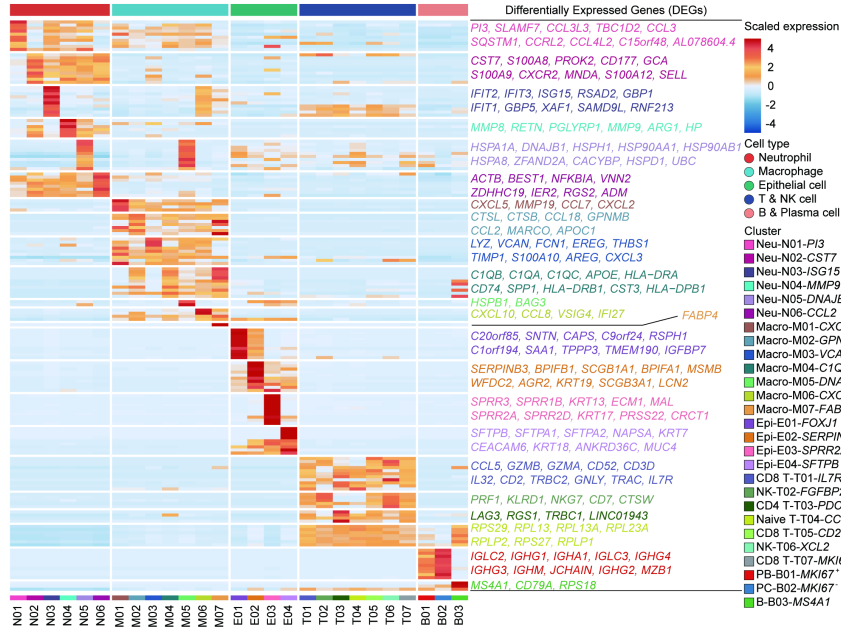


Figure 3

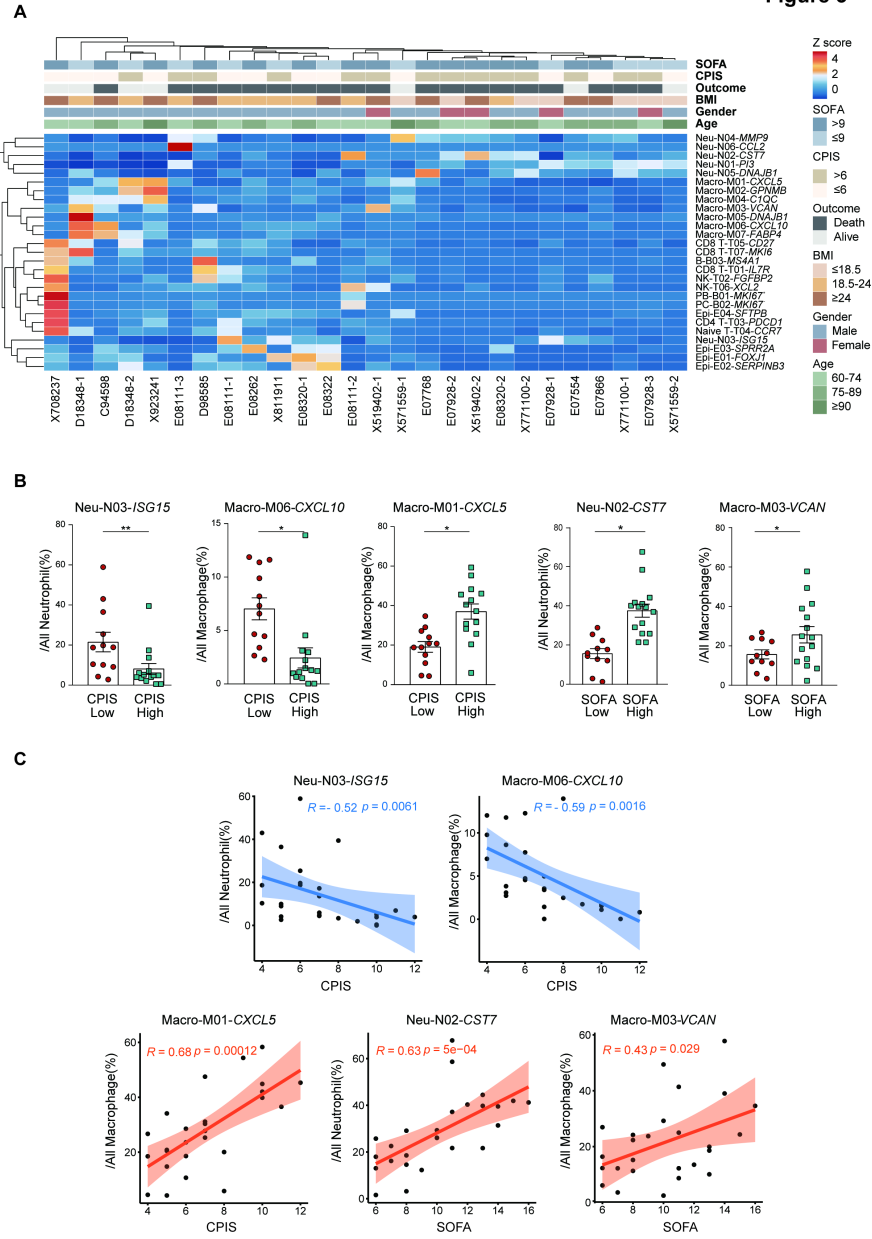


Figure 4

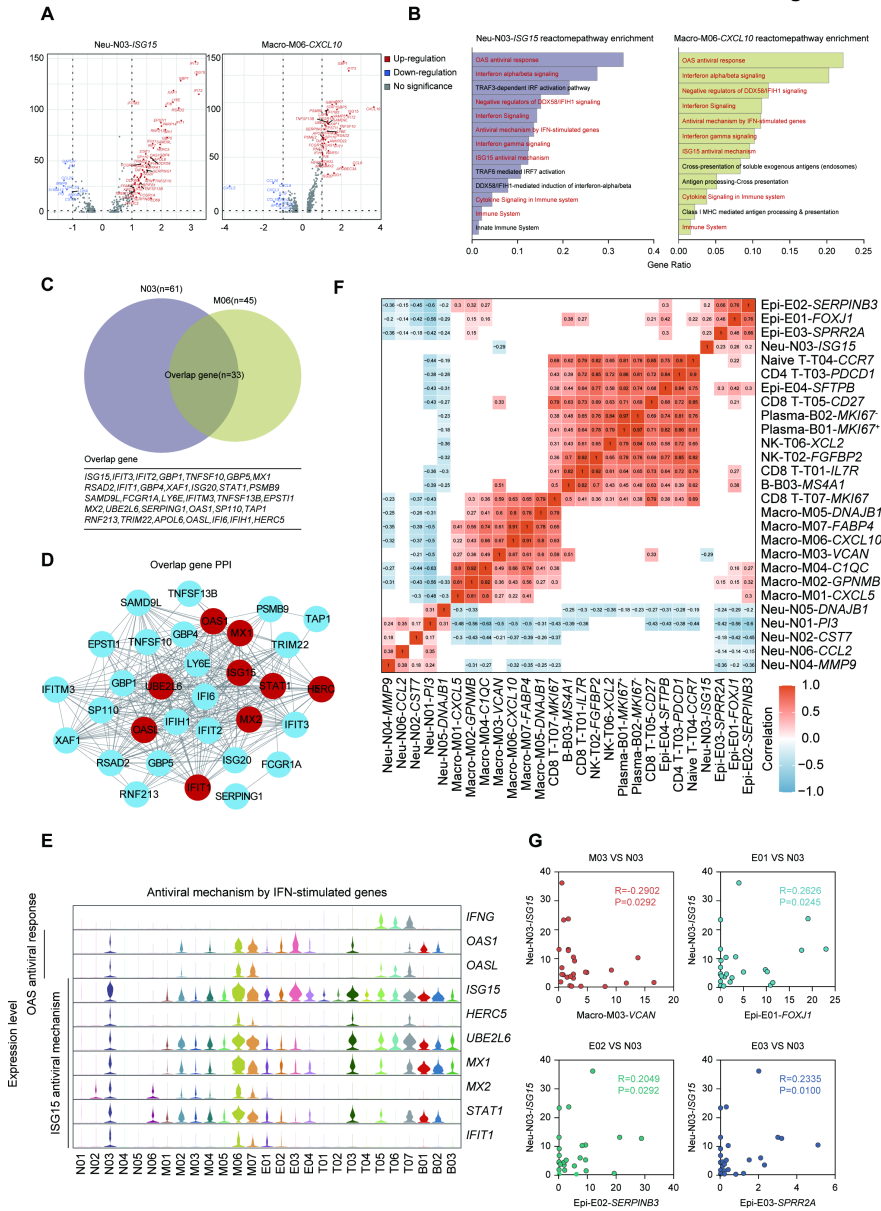


Figure 5

